EUROFUSION WPS2-PR(15) 14533

F Warmer et al.

On the Characterisation of the Edge Ion Energy-Flux in Advanced Stellarators

Preprint of Paper to be submitted for publication in
Nuclear Fusion

This work has been carried out within the framework of the EUROfusion Consortium and has received funding from the Euratom research and training programme 2014-2018 under grant agreement No 633053. The views and opinions expressed herein do not necessarily reflect those of the European Commission.

On the Characterisation of the Edge Ion Energy-Flux in Advanced Stellarators

F. Warmer[a,*], P. Xanthopoulos[a], C.D. Beidler[a], H. Maaßberg[a], R. Wolf[a]

[a] *Max Planck Institute for Plasma Physics, D-17491, Greifswald, Germany*

Abstract

Due to the reduction of neoclassical transport in optimised stellarator configurations, it is expected that turbulence will significantly contribute to the heat and particle transport – at least in the edge region of the plasma – and may thus pose a limit to the achievable confinement and performance of such machines. In order to predict the confinement and develop plasma scenarios for W7-X and beyond for Helias reactors in an efficient way, it is important to develop models which can describe the characteristics of turbulent transport using only a fraction of the computational power which is normally required for gyrokinetic simulations on petaflop scale.

In this work we concentrate on the ion-temperature-gradient mode which has so far been well investigated and is considered to strongly contribute to transport. Non-linear full-flux surface gyrokinetic simulation results are compared for W7-X and its predecessor W7-AS. Although the fluctuations are more localised in W7-X, it is intriguing that the normalised heat flux scaling is nearly identical.

On this basis experimental results from W7-AS are reviewed which suggest that the critical gradient behaviour of the ITG mode indeed dominates the edge transport. As the experimental and theoretical obtained characteristics are similar a basic ITG critical gradient model is proposed and verified in 1-D transport simulations against the W7-AS experimental results showing good agreement.

The model is therefore further applied to W7-X showing, that even with ITG transport the a global confinement enhancement with respect to the ISS04 scaling of $\tau_E^{1D}/\tau_E^{\mathrm{ISS04}} = 1.7$ is retained. Extrapolation to a Helias reactor scenario shows similar promising results with an confinement improvement factor of 1.35. However, the overall transport is sensitive to the 'stiffness' used in ITG model. In future works it is envisaged to enhance the model by taking into account the density gradient and radial electric field which was so far neglected, but are both considered to reduce the turbulence level of the ITG.

Keywords: HELIAS, Transport modelling, Ion temperature gradient mode

1. Introduction

A key property for the success of fusion power plants is the confinement of the plasma energy and particles. The tokamak demonstrates good confinement over a wide range of experimental devices, and this success triggered the ITER project [1], a large tokamak reactor under construction in France, designed to achieve a significant amount of fusion power. Despite this encouraging feature, tokamaks suffer from disruptions and plasma instabilities driven from the internal current, thus limiting their performance. In addition, tokamaks are difficult to operate in steady-state, ensuing very high demands on the control system.

The stellarator concept, on the other hand, is by construction free of all of the above mentioned drawbacks. However, the first stellarator experiments demonstrated a relatively poor confinement attributed to particles 'trapped' in certain unfavorable locations of the complicated magnetic field. In modern optimized stellarators of the Helias-type this issue is overcome thanks to a sophisticated three-dimensional shaping of the magnetic field. This optimization principle will be validated by the Wendelstein 7-X (W7-X) experiment [2], planned to start operation in late summer 2015.

With the drastic improvement of trapped-particle confinement in advanced stellarators, however, transport losses induced by turbulence will inevitably play a significant role. Due to its strong temperature dependence, neoclassical transport is expected to be still the dominant driver of transport in the centre of the plasma, especially in high temperature discharges, but as the temperature decreases strongly towards the plasma edge, neoclassical transport is reduced and turbulent transport becomes important. Already in Wendelstein 7-AS (W7-AS) [3], the predecessor of W7-X, it was shown that turbulent losses overcomes the neoclassical transport in the outer third of the minor radius.

In this context, renewed attention is focused on the prospects of optimized stellarators as fusion power plants. However, in order to assess the size and performance of such devices, an accurate prediction of the plasma transport is required, which crucially affects confinement. So far such predictions were achieved by employing empirical confinement time scalings. These estimations, despite their realistic merit – being obtained by regression from a large database of various stellarators worldwide [4] – are hardly adequate for studies on optimized configurations [5]. In these devices plasma turbulence is expected to play an important role perhaps even overcoming the neoclassical transport which dominates in existing stellarator experiments.

While many well-validated codes and tools have been developed in the course of stellarator research for the prediction and analysis of the neoclassical transport effects [6], the treatment of turbulence in 3D magnetic fields has only recently been started [7]. So far, complex gyrokinetic codes are used to investigate turbulent behaviour in stellarators which require peta-flop scale supercomputers to run. But in order to prepare operation of high-performance discharges of W7-X efficiently, predictive capability of turbulent transport is required on a small computational scale. Such a development is the topic of this paper with concentration on the ion energy flux induced by the ion-temperature-gradient instability (ITG).

In section 2 indications and features of ITG transport from gyrokinetic simulations of W7-X and W7-AS are presented.

*Corresponding author, Tel.: +49 (0)3834 88-2583
Email address: Felix.Warmer@ipp.mpg.de (F. Warmer)

The similarity of the ITG behaviour between those two devices is highlighted and these theoretical results are complemented by W7-AS experimental results. On the basis of the qualitative agreement between theory and experiment in section 3 a basic model for the ITG induced ion energy flux is presented compatible with a neoclassical transport code. Application of the code to W7-AS leads to good agreement. Consequently the model is also applied for W7-X in section 4, where for the first time a predictive transport scenario is shown for W7-X with integrated neoclassical and turbulent transport. As still several uncertainties remain in this approach the section is concluded by sensitivity analysis of W7-X confinement with respect to parameter variations in the basic ITG model. Beyond that, the model is also applied for a reactor scenario of the Helias line in section 5. The various results and implications of the work are discussed and summarised in section 6.

2. Turbulence in Advanced Stellarators

In tokamaks and smaller stellarator experiments, two important microinstabilities in fusion plasmas are the ion-temperature-gradient (ITG) mode and the trapped-electron-mode (TEM), both of which can significantly contribute to plasma transport and are consequently of relevance for predictive transport modelling. In this paper, however, which attempts to include for the first time physics-motivated turbulence models for transport prediction, only the ITG mode is considered. The TEM is going to be neglected in this initial approach for the following reasons:

In a quasi-isodynamic stellarator like W7-X, it has been found that the unfavorable curvature which excites the TEM instability is spatially separated from the trapping region of the particles [8]. In W7-X the trapped particles are mainly located in the straight regions of each field period, i.e. in the triangular plane, where they precess poloidally. The unfavorable curvature, in contrast, is located at the corners of the straight field, i.e. in the bean-shaped plane of the configuration. This separation of trapping and curvature leads to a reduced transport from the TEM compared to tokamaks, in which those regions generally overlap.

Moreover, in quasi-isodynamic configurations with the so-called 'maximum-J' property (the parallel adiabatic invariant J attains its maximum on the magnetic field axis, while monotonically decreasing towards the edge), it can be analytically shown that collisionless TEMs are stable over a large parameter range [9]. An electron displaced by the density gradient would need to gain energy in order to conserve J (for $\partial J/\partial r < 0$) thus tapping energy from the instability. Consequently in a quasi-isodynamic maximum-J configuration any electrostatic instability would be stabilised by the electrons. Of course, both quasi-isodynamicity and maximum-J can in reality only achieved to a certain degree, but advanced stellarators like W7-X approach these properties adequately. This is confirmed by gyrokinetic simulations of TEMs for W7-X where it was found that the energy flux is an order of magnitude lower in W7-X than in the DIII-D tokamak [10].

In this work the properties of ITG-induced transport in W7-X are reviewed and new results for W7-AS are presented. The ITG features of both devices are compared and complemented by W7-AS experimental results.

2.1 Indications for ITG-induced Transport from Gyrokinetic Simulations

It is well known from tokamaks how temperature gradient driven instabilities have strong impact on the plasma transport leading to so-called profile stiffness. When the temperature gradient exceeds a critical threshold, the transport in tokamaks is observed to increase severely thus holding the temperature gradient at its critical value. The temperature profile is therefore independent of any heating scheme and the temperature which can be reached is nearly only determined by the boundary condition. In tokamak H-mode, the edge develops a so-called pedestal which shifts the stiff temperature profile as a whole towards higher temperatures by a sharp increase of the edge temperature.

But so far, neither profile stiffness nor pedestals have been observed in stellarator experiments. In the absence of a plausible assumption for the temperature profile, it is advisable to conduct a theoretical investigation of ITG-induced turbulence in stellarators using a numerical gyrokinetic formulation. In tokamaks, it is usually sufficient to simulate a single flux tube to determine the transport on a flux surface, as thanks to axisymmetry, all flux tubes are identical. In stellarators, in contrast, different flux tubes are not geometrically equivalent, thus requiring the simulation of the entire flux surface to determine quantitatively the transport level. For this purpose, the gyrokinetic code GENE [11, 12] was employed, which is capable of treating an entire flux surface of any toroidal configuration [13], while maintaining the local approximation in radial direction.

The results of a full flux surface GENE simulation for W7-X is illustrated in Fig. 1 [14]. The turbulence is driven by the ion temperature gradient (the density profile is considered flat) for gyrokinetic ions and Boltzmann distributed electrons.

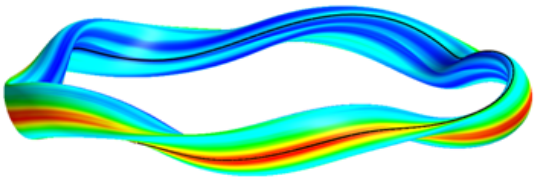

Figure 1: ITG induced root-mean-squared electrostatic potential fluctuations of a full flux-surface GENE simulation of Wendelstein 7-X [14].

As can be seen from Fig. 1, a remarkable stellarator-specific outcome is that the strongest turbulent fluctuations are located on a thin band on the outboard side of the flux surface while the remaining surface is relatively quiescent. This is in strong contrast to tokamaks where typically the full outboard side is dominated by strong fluctuations. Thus, it has been identified that the variation of the curvature on a flux surface in a stellarator such as W7-X causes the localisation of the turbulent fluctuations. This localisation in turn affects the scaling of the energy transport with respect to the gyroradius normalized to the minor radius, $\rho^* = \rho_i/a$. As ρ^* takes larger values, the transport stiffness is decreasing as seen in Fig. 2, unlike the standard gyro-Bohm scaling found in tokamak experiments and gyrokinetic simulations. In the limit $\rho^* \to 0$, the stiffness converges to a maximum value which can be regarded as the worst

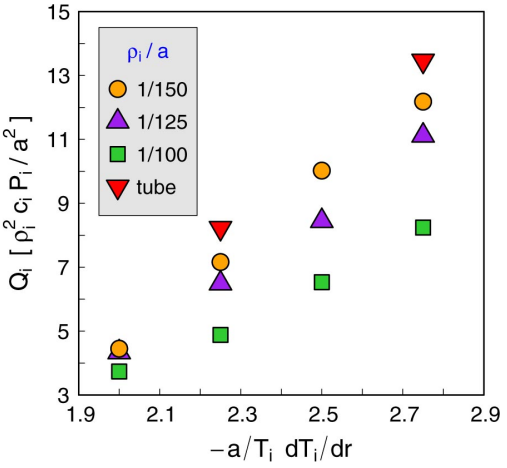

Figure 2: Normalised heat flux density over the ion temperature gradient for non-linear full flux surface GENE simulations of W7-X for three different values of the normalised ion gyroradius $\rho^* = \rho_i/a$. Results from simulations of the most unstable flux tube are shown for comparison [14].

case in view of the ITG mode and thus the stiffness becomes independent of ρ^*, which will be important for the comparability of W7-AS and W7-X in the next subsection.

2.2 Comparison of W7-AS and W7-X

In order to clarify if conclusions about W7-X can be extrapolated from its predecessor W7-AS, similar non-linear full flux surface gyrokinetic simulations for W7-AS had to be carried out as well. The resulting time-averaged root-mean-squared electrostatic potential fluctuations are for both devices compared in Fig. 3. It turns out that there is some qualitative difference in the poloidal distribution of the fluctuations. While the fluctuations for W7-X are quite localised in a small band on the outboard side, for W7-AS the fluctuations are somewhat more broadly distributed. Still, the fluctuations in W7-AS are stellarator-specific compared to tokamaks where the full outboard side has equally high fluctuations. Also, the fluctuations distribution in W7-AS is similar to other investigated quasi-omnigenous stellarator configurations such as MPX which showed a similar pattern [14].

Despite this difference, the question arises if the unique fluctuation pattern has some impact on the heat flux. To answer this, the heat flux density is compared for W7-X and W7-AS in Fig. 4. The heat flux density is thereby normalised to the gyro-Bohm value

$$Q_{gB} = \frac{\rho_i^2 v_{Ti} p_i}{a^2} \tag{1}$$

where ρ_i is the ion gyroradius, v_{Ti} the thermal speed, p_i the ion pressure and a the minor radius of the machine. The simulations were done at the radial location where the normalized toroidal flux takes the value $s = 0.5$, ignoring the density and electron temperature gradients. In addition, the radial electric field was not taken into account. The normalised temperature gradient a/L_{Ti}, being the driving factor of the ITG mode, has been varied between 2 and 2.75 in order to compare the stiffness of both configurations.

As has been pointed out in the last subsection, the stiffness depends on the normalised gyroradius if its value is larger than $\rho^* > 150$. Therefore, both for W7-X and W7-AS a very small ρ^* was chosen, such that one can assume the results of the stiffness presented in Fig. 4 to be independent of ρ^*. This is important in order to be able to compare the stiffness in these simulations for both devices as this limit represents the absolute worst case for either configuration, thus ensuring comparability.

Moreover, it must be clarified if the heat flux density, normalised to gyro-Bohm units, is indeed a suitable figure of merit, as one has to keep in mind, that W7-X is over a factor three larger than W7-AS. The total power crossing the flux surface is

$$P = \int \frac{Q \cdot \nabla r}{|\nabla r|} dS = A \langle Q \cdot \nabla r \rangle \tag{2}$$

where $\langle \ldots \rangle$ represents the flux surface average and $A = V'(r)$ is the radial derivative of the volume enclosed by the surface. The total power crossing the flux surface thus becomes

$$P = \rho_i^2 v_{Ti} p_i \frac{A}{a^2} \widehat{Q} \tag{3}$$

where $\widehat{Q} = \langle Q \cdot \nabla r \rangle / Q_{gB} = Q_i / Q_{gB}$ is the normalized heat flux density as shown in Fig. 4. Consequently, if the local plasma parameters at the edge are assumed to be the same both in W7-AS and W7-X, the total power crossing the flux surface must be modified by the geometrical factor A/a^2. But this factor is nothing more than the aspect ratio $\widetilde{A} = R/a$ and some equal constant factor. As the aspect ratio equals $\widetilde{A} \approx 10$ for both devices, the total power crossing the separatrix P will also be almost the same, for similar local plasma parameters and heating power.

It follows that for similar plasma parameters and heating power, the ITG induced heat flux density is a factor 10 lower in W7-X than W7-AS. This result could be checked in W7-X experiment employing about 1 MW NBI heating with a density of about $1 \cdot 10^{20}$ m^{-3} in the centre.

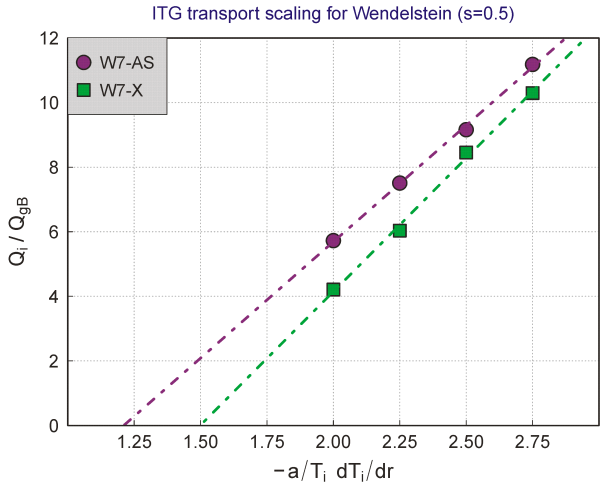

Figure 4: Normalised heat flux density over the ion temperature gradient for non-linear full flux surface GENE simulations of W7-X ($\rho^* = 1/400$) and W7-AS ($\rho^* = 1/150$).

Interestingly, the scaling of the normalised heat flux density is very similar for both W7-X and W7-AS in the local limit.

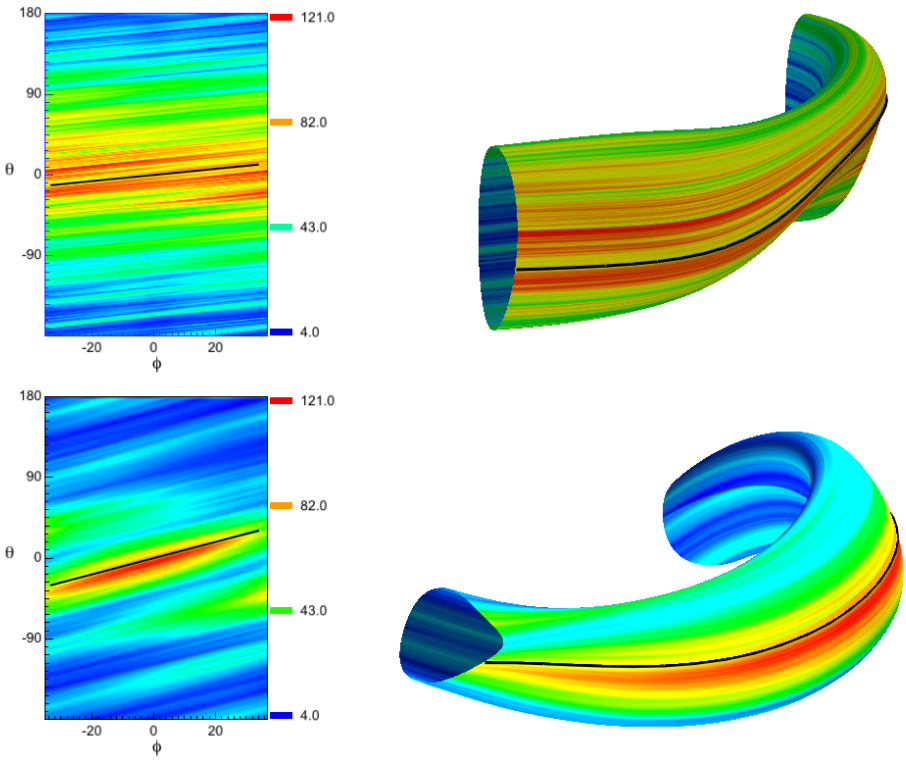

Figure 3: ITG induced root-mean-squared electrostatic potential fluctuations of a full flux-surface GENE simulation of W7-AS (top) and W7-X (bottom).

The critical gradient length is for W7-X slightly shifted upwards with $(a/L_{Ti})^{ITG}_{crit} = 1.5$ compared to 1.25 for W7-AS. The stiffness, i.e. the linear increase of the heat flux density with increasing ion temperature gradient length, is nearly identical. This favorable similarity allows to employ existing experimental results from W7-AS, in order to predict salient transport properties for W7-X, as presented in the following.

2.3 W7-AS Experimental Results

The results of the gyrokinetic simulations suggest that, under certain scenarios involving NBI heating, transport from ITG turbulence could play a significant role in advanced stellarators. In the following, the experimental data from W7-AS is investigated with respect to ITG-like transport. For such a study two well documented high performance discharges of W7-AS, #34609 and #34313, are selected, which have been analysed in terms of neoclassical transport [15]. The profiles for the discharge #34609 are shown in Fig. 5. The corresponding profiles for the discharge #34313 are similar with about half the density in the centre compared to #34609.

It can be seen from Fig. 5, that a clear discrepancy arises between the experimental, Q_i^{exp}, and the neoclassical ion energy flux, Q_i^{neo}, in the outer region of the minor radius $r > 2/3a$ of the presented discharges. This indicates that, apart from neoclassical transport, other transport mechanisms must determine the energy flux at the edge.

In order to assess the contribution of ITG turbulence to the overall transport, the driving factor, namely the normalised temperature gradient

$$\frac{a}{L_{Ti}} = -a \cdot \frac{|\nabla T_i|}{T_i} \qquad (4)$$

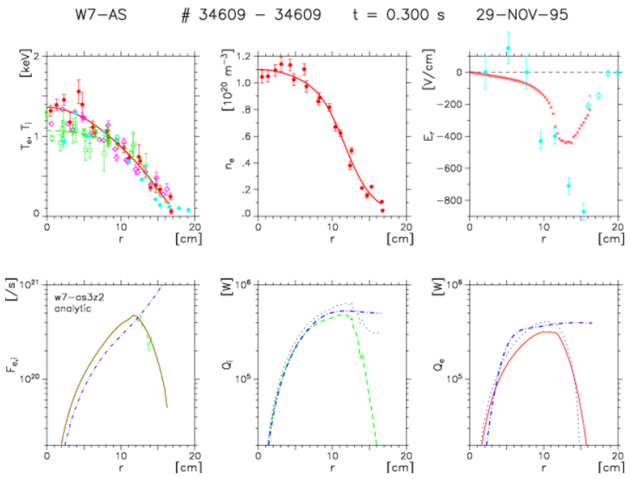

Figure 5: Temperature, density and radial electric field profiles (top) for the W7-AS discharge #34609 and comparison of the experimental and the corresponding neoclassical particle and energy fluxes (bottom).

is plotted as function of the minor radius in Fig. 6.

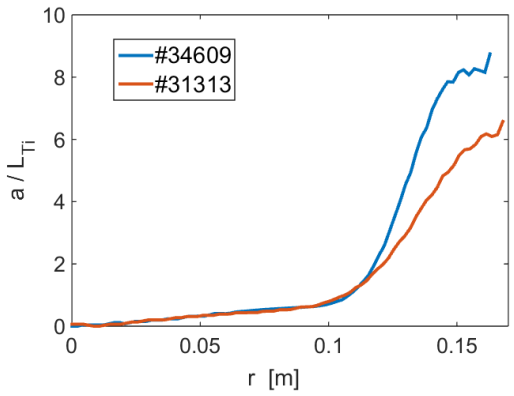

Figure 6: Normalised ion temperature gradient over the minor radius of the experimental results from W7-AS for #34609 and #34313.

The normalised temperature gradient increases for both #34609 and #34313 sharply in the outer third of the minor radius which coincides with the region where the neoclassical and experimental ion energy flux deviate. Moreover, a/L_{Ti} towards the edge is far above the critical gradient, which is on the order of $a/L_{\mathrm{crit}} \approx 2$. It is thus very likely that the edge ion energy flux of the presented cases of W7-AS is driven by ITG-like transport.

From a scale separation argument one can argue that neoclassical and turbulent energy fluxes are additive, thus one can define the residual energy flux Q_i^{res} derived from the experimental profiles as

$$Q_i^{\mathrm{res}} = Q_i^{\mathrm{exp}} - Q_i^{\mathrm{neo}}. \tag{5}$$

As this residual energy flux is here speculated to be driven by ITG turbulence, in the following the residual energy flux is related to the normalised temperature gradient, see Fig. 7.

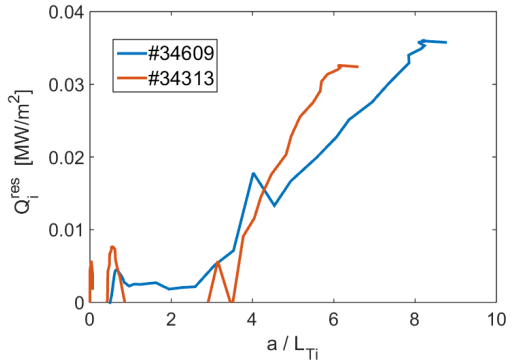

Figure 7: Residual edge ion energy flux as function of the normalised temperature gradient of the experimental results from W7-AS for discharges #34609 and #34313.

Here, a clear correlation between the residual edge ion energy flux and the normalised temperature gradient is observed. In addition, the typical critical gradient behaviour of ITG-like transport is apparent, as found in the full flux surface GENE simulations.

The total residual ion energy flux is comparable in both discharges, although the central density is a about factor two different. The normalised density gradient length is also comparable in both discharges, reaching large values towards the edge. A notable feature found in Fig. 7 is the existence of a critical gradient, above which the residual ion energy flux increases strongly. For both discharges this critical gradient is in the same range of $(a/L)_{\mathrm{crit}} \approx 2$ which is slightly higher than the value obtained from the GENE simulation for W7-AS with 1.25.

It is not completely clear why the energy flux increases more strongly for the discharge #34313 than #34609. As the profiles investigated here are fits to the experimentally scattered data it is possible that the difference in the stiffness of the residual edge ion energy flux in both discharges comes from a misalignment of the fit with the experimental, especially as the edge temperature is very low and the relative error thus high. Another reason may be that the heating power in #34313 is about 20 % higher which may cause the transport to increase accordingly.

3. The Transport Model

Following a widely used practice in the tokamak community, in the following we we introduce an ITG energy flux model which embeds the basic features of the ITG transport in Helias-type configurations and can be used for transport estimations based on simulations and existing experimental results alike. We should mention that a similar approach has also recently been proposed for the LHD experiment combining fits from linear ITG growth rates and the zonal flow (ZF) residual levels [16]. This approach, although quite successful for LHD, would not be applicable to W7-X. For instance, it has been shown that the dynamic as well as the long term ZF behavior is entirely different in the two devices, due to the distribution of trapped particles.

The contribution of anomalous transport in W7-AS has historically been expressed via a speculative rule following the inverse plasma density, also involving a fudge factor [17, 18]. In this work, we concentrate instead on the ITG critical gradient model, in which the energy flux is directly related to the driving gradient. Below criticality, no heat flux is assumed, while beyond that threshold the heat flux is expected to quickly grow. As demonstrated by the non-linear gyrokinetic simulations, see Fig. 2, such a relation can very well be described by a linear relation. In its most basic form we can describe these features with the expression

$$Q_i^{\mathrm{ITG}} = w \cdot y \cdot H(y), \tag{6}$$

where w is the linear increase, from here on called 'stiffness', y the normalised temperature gradient minus the critical value:

$$y = \frac{a}{L_{Ti}} - \left(\frac{a}{L_{Ti}}\right)_{\mathrm{crit}} \tag{7}$$

and H is the Heaviside function to ensure that the energy flux is zero below marginality. The model in this form has thus two free parameters, the stiffness w and the critical gradient $(a/L_{Ti})_{\mathrm{crit}}$, which need to be determined.

For the analysis of the neoclassical transport, it is assumed that the plasma may be described by local approximation to solve the drift kinetic equation. Consequently all quantities are

assumed to be constant on flux surfaces such that the plasma is described only in one dimension by the flux surface label ψ. The transport code [19, 20] solves the power balance for the electrons and ions and the neoclassical ion energy flux is as usual expressed as

$$Q_i^{\mathrm{neo}} = -n_i T_i \left[D_{21}^i \left(\frac{\nabla n_i}{n_i} - \frac{Z_i E_r}{T_i} \right) + D_{22}^i \frac{\nabla T_i}{T_i} \right] \qquad (8)$$

where the thermal transport coefficients D_{ij} are obtained by the appropriate energy convolutions with the local Maxwellian distribution function and the mono-energetic diffusion coefficients. A database of the mono-energetic diffusion coefficients is prepared in advance for each magnetic configuration using the DKES code [21, 22]. The radial electric field E_r is obtained by solving the ambipoarity constraint $Z_i \Gamma_i = \Gamma_e$ where Z_i is the charge number and $\Gamma_{i,e}$ the particle fluxes of ions and electrons, respectively.

In our approach here, the total ion energy flux considered in the power balance is according to the scale separation argument the sum of the neoclassical part and the ITG energy flux:

$$Q_i = Q_i^{\mathrm{neo}} + Q_i^{\mathrm{ITG}} \qquad (9)$$

The neoclassical transport of the electrons is modeled in the same way as for the ions, while the 'anomalous' transport of the electrons is modeled as

$$Q_e^{\mathrm{ano}} = -\chi_e^{\mathrm{ano}} n_e \nabla T_e \qquad (10)$$

where the anomalous heat conductivity $\chi_e^{\mathrm{ano}} \sim n^{-1}$ has been derived empirically from a regression over a wide range of experimental data from W7-AS [17, 18]. A more physics motivated model, as has been proposed for the ITG transport, will be the subject of a future study. In the next step, the transport model shall be applied to the W7-AS experimental data with focus on the ion energy flux in order to verify the applicability of the proposed ITG critical gradient model.

3.1 Verification against W7-AS Data

For the preparation of the W7-AS simulations in the first step a database of mono-energetic transport coefficients must be created. This has been done with DKES employing the W7-AS vacuum configuration. In the experimental discharges of relevance here, the full field was used with $B_t = 2.5$ T, thus the plasma beta was very low, on the order of $\beta = 0.5$ %. The vacuum configuration turns out therefore to be a good approximation in order to calculate the neoclassical transport coefficients.

For the simulations the density profile is used as input and kept constant since we are not interested in transient behaviour and not enough information is available to model a complete fuelling scenario. The plasma heating is also taken constant, and modelled according to the calculated absorption profiles from which the radiation from impurities is directly subtracted.

The anomalous electron heat conductivity is adjusted such as to reach the same value at the edge as in the experimental data with $\chi_e^{\mathrm{edge}} = 1.6$ m^2/s.

As the transport model solves a set of coupled diffusion equations, the required boundary conditions play an important role. Both the edge ion and electron temperatures are set at $T_{i,e} = 0.1$ keV in agreement with the experimental values.

Finally the two free parameters of the ITG critical gradient model are adjusted according to the experimental observations. With these inputs the integrated 1-D simulations are conducted, and the temperature profiles, the energy fluxes as well as the radial electric field are calculated self-consistently. The simulation results for discharge #34609 are compared to the experimental results of W7-AS in Figs. 8, 9 and 10.

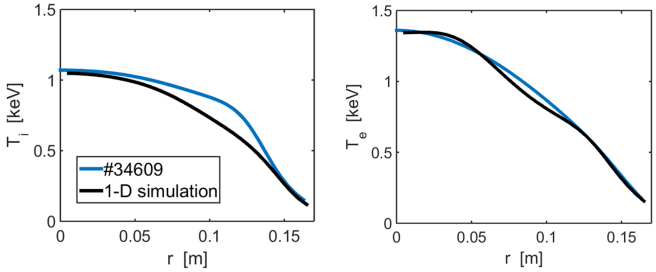

Figure 8: Results for the ion and electron temperature from the 1-D simulations with the ITG critical gradient model (black) in comparison with the experimental results from W7-AS for #34609 (blue).

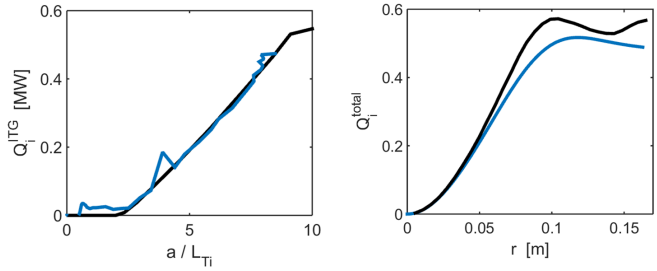

Figure 9: Results for the ion and electron temperature from the 1-D simulations with the ITG critical gradient model (black) in comparison with the experimental results from W7-AS for #34609 (blue).

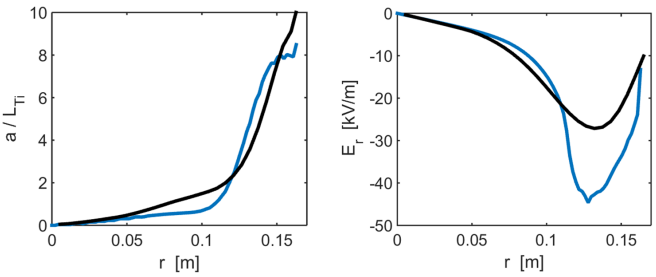

Figure 10: Results for the ion and electron temperature from the 1-D simulations with the ITG critical gradient model (black) in comparison with the experimental results from W7-AS for #34609 (blue).

There is generally good agreement found between the 1-D simulation and the experimental W7-AS results. The calculated temperature profiles match adequately the experimental profiles. Only the ion temperature profile deviates somewhat in the transition region around $r = 0.1$ m where the plasma transport changes from neoclassically driven towards being dominated by anomalous transport. Interestingly, the near-axis as

well as the edge regions are in very good agreement. It is unlikely that the ITG model is responsible for this deviation as the anomalous transport really starts to a play role for $r > 0.1$ m. Fig. 9 shows that the critical gradient behaviour is captured well by the ITG model and the total ion energy flux is in good agreement with experiment. Only at the very edge does the model seem to slightly overestimate the energy flux. This can be understood from the right side of Fig. 10 which shows that the ion temperature gradient deviates from the experimental values, being somewhat larger at the edge thus leading to increased energy flux. This is most likely caused by the boundary condition since only small changes of the edge temperature directly influence the edge temperature gradient. Although the radial electric field is not explicitly included in the model, it is in agreement with experiment.

Recalling the experimental data, Fig. 5, one recognises that there is rather strong scattering of data points in the region around $r = 0.1$ m. Nonetheless, the agreement between simulation and experiment is well within experimental accuracy.

It can be concluded that the ITG critical gradient model is indeed suited to capture the basic features of the anomalous transport observed in the W7-AS experiment and moreover allows a quantitative assessment of the ion energy flux. In the next step this modelling approach shall be applied to a W7-X scenario, where reference parameters for the stiffness and the critical gradient are derived from a combination of the W7-AS experimental values and the gyrokinetic results.

4. Transport Prediction for W7-X

Similar with W7-AS, several general inputs need to be defined in order to carry out the W7-X simulations. First, for the preparation of the DKES database, the so-called 'standard case' magnetic configuration of W7-X has been selected with a finite plasma beta of $\beta = 2$ %. Although W7-X has been optimised for a small Shafranov shift, the magnetic field is still modified by a finite beta, which has impact on the neoclassical transport coefficients.

For the density a 'standard' profile has been selected and kept constant again to avoid a fuelling scenario which requires detailed knowledge of particle sources and sinks. In fact, density control in large stellarators is generally problematic and requires central sources such as pellet injection to avoid hollow density profiles [23]. However, this is beyond the scope of this work, but wil be investigated in future studies.

Regarding the anomalous electron transport, as so far no better quantitative assessment exists, the anomalous electron heat conductivity has been set to $\chi_e^{\rm edge} = 1.6$ m^2/s at the very edge and falling off towards the centre at a rate $\chi_e^{ano} \sim 1/n$, in line with the W7-AS experimental data.

4.1 Reference Scenario

In the reference scenario, the heating scheme is chosen to be neutral beam injection (NBI), which is necessary to effectively heat the ions and thus bring the ion temperature to a maximum value which in turn leads to a significant ion temperature gradient. Consequently the heating power of the NBI has been chosen very high at 9 MW absorbed power. Such a heating scenario is not only most relevant for the investigated ITG mode, but also most relevant for future reactor scenarios where $T_i \approx T_e$.

For the ITG model the same value for the critical gradient has been used as found in the experimental discharge #34609. The stiffness, however, had to be modified according to the used normalisation. Starting from equation 3, as $\widehat{Q}_{\rm W7AS} \approx \widehat{Q}_{\rm W7X}$, the ITG heat flux density of W7-X can be expressed in terms of W7-AS as

$$Q_i^{\rm W7X} = \left(\frac{a_{\rm W7AS}}{a_{\rm W7X}}\right)^2 \cdot \frac{P_{\rm W7X}}{P_{\rm W7AS}} \cdot Q_i^{\rm W7AS} \tag{11}$$

where the local plasma parameters have been accordingly substituted with the heating power P in order to be consistent with the global power balance. The heat flux density for W7-AS can now be replaced by the ITG critical gradient model taking for the free parameters the values obtained from the experimental data:

$$Q_i^{\rm W7X} = \left(\frac{a_{\rm W7AS}}{a_{\rm W7X}}\right)^2 \cdot \frac{P_{\rm W7X}}{P_{\rm W7AS}} \cdot w_{\rm W7AS} \cdot y \cdot H(y) \tag{12}$$

with

$$y = \frac{a}{L_{Ti}} - \left(\frac{a}{L_{Ti}}\right)_{\rm crit}^{\rm W7AS}. \tag{13}$$

The stiffness parameter to employed for the W7-X simulations is consequently

$$w_{\rm W7X} = \left(\frac{a_{\rm W7AS}}{a_{\rm W7X}}\right)^2 \cdot \frac{P_{\rm W7X}}{P_{\rm W7AS}} \cdot w_{\rm W7AS} \approx 1.0 \cdot w_{\rm W7AS}. \tag{14}$$

This is of course only true under certain assumptions. First, we assume that the effect of the finite gyroradius, density gradient and radial electric field have a similar impact on both configurations Secondly, the local plasma parameters at the edge must be similar according to equation 3. Consequently, the Dirichlet boundary condition for the temperature has been set to $T_{i,e} = 0.1$ keV which corresponds to the experimental values from W7-AS.

In this context, equation 3 also explains why we do not expect a much higher edge temperature (something like a pedestal) in W7-X. Reformulating equation 3 in terms of temperature one obtains

$$P \sim n_i T_i^{5/2} \widehat{Q}. \tag{15}$$

Although the heating power is a factor 10 higher in W7-X than in W7-AS, the strong temperature scaling indicates that the edge temperature may not increase much more than a factor two from 0.1 to 0.2 keV at the edge.

Results for the 1-D predictive transport simulation including the ITG model using W7-AS parameters are presented in Fig. 11.

The most striking result of this predictive simulation is the fact, that the improvement of the global confinement with respect to the empirical ISS04 scaling is retained. In this reference case using the W7-AS parameters for the stiffness of the ITG transport, the confinement improvement is $f_{\rm ren} = \tau_E/\tau_E^{\rm ISS04} = 1.7$ reaching a volume averaged beta of $\langle\beta\rangle = 2.4\%$ and central temperatures of about $T_{e,0} \approx T_{i,0} = 4$ keV. In the present methodological context, these results are very promising suggesting a very good global confinement for W7-X.

In the next subsection we assess the sensitivity of the global confinement with respect to variations in the parameters introduced for the ITG critical gradient model.

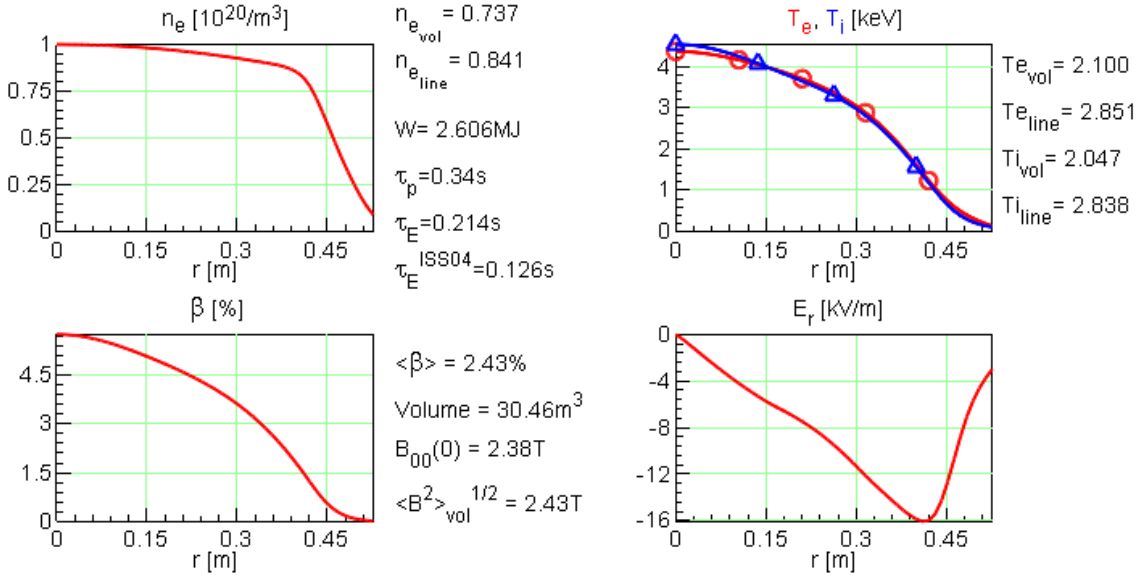

Figure 11: Profiles for the density (top left), temperature (top right), plasma beta (bottom left) and radial electric field (bottom right) for the 1-D predictive transport simulation of the W7-X 'reference' scenario with 9 MW absorbed NBI heating power, 0.1 keV edge temperature and experimental W7-AS parameters for the ITG model.

4.2 Sensitivity Analysis

One of the most crucial parameters on the confinement, also known from tokamaks, is the stiffness. Therefore, in the following the sensitivity of the global confinement of W7-X with respect to variations in the stiffness of ITG model shall be investigated. For this purpose the above described predictive transport simulations of W7-X have been repeated both with smaller and higher stiffness compared to the reference scenario while keeping the critical gradient at the same value. The corresponding results are shown in Fig. 12.

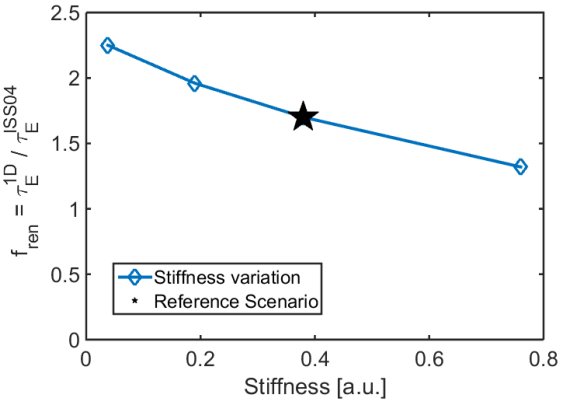

Figure 12: Sensitivity of the confinement time normalised to the emiprical ISS04 scaling with respect to the variation of the stiffness of the ITG model in the 1-D simulations. The reference scenario is displayed in the middle.

A considerable increase of the stiffness by a factor two leads to strong degradation of the confinement from $f_{\rm ren} = 1.7$ down to 1.4. Still, the global confinement stays well above the ISS04 empirical scaling retaining the generally good confinement properties of W7-X. A reduction of the stiffness by a factor two strongly increases the global confinement to $f_{\rm ren} = 1.9$. The confinement continues to increase with further reducing the stiffness to $f_{\rm ren} = 2.2$ for a marginal level of stiffness.

The variation of the critical gradient length a/L_{Ti}, on the other hand, does not impact the confinement at all in the predictive simulations. Generally the stiffness in advanced stellarators is not so pronounced – quite in contrast to tokamaks. Consequently, also the critical gradient in the predictive simulations does not play a significant role. Due to the rather low stiffness, the ion temperature profile becomes very steep towards the edge, as has been shown in subsection 2.3 from the W7-AS experimental data. Those gradients are much larger than the critical gradient. If the critical gradient is reduced, the ITG transport start to act closer to the centre, where the neoclassical transport dominates.

The boundary condition for the edge temperature has not been varied to a great degree since an increase of the edge temperature strongly increases the ITG heat flux which in turn should lead again to a temperature reduction. This is in line with existing experimental data from stellarators worldwide which so far did not observe pedestal structures as known from tokamaks.

The final variation has been done for the heating scheme. For this, the reference scenario was modified to use 9 MW absorbed ECRH power instead of NBI. In this case the confinement improvement with respect to the ITG model is clear. The ECRH is affecting mainly the electrons and the ion temperature stays rather low and consequently also the gradients. As the ITG heat flux is mainly driven by the gradients, the ITG transport is reduced and the confinement increased which reaches $f_{\rm ren} = 2.8$ compared to $f_{\rm ren} = 1.7$ for the reference case. However, this result is obtained for a fixed value of the anomalous

electron heat conductivity. In reality it is probable that the anomalous electron heat flux increases with increasing electron temperature gradient and the confinement improvement of the ECRH case compared to the reference NBI case would be less than predicted here.

This sensitivity study shows, that even if the stiffness in the presented approach is underestimated, the prediction for the improvement of the W7-X plasma confinement with respect to the ISS04 scaling holds. Unless the anomalous electron transport is also substantially underestimated or other transport channels become apparent, the predictive transport simulations for W7-X are promising.

5. Extrapolation to Helias Reactor

In order to carry out predictive transport simulations of a Helias reactor, a suitable magnetic configuration has to be defined. As dedicated reactor configurations are still a topic of ongoing research, the existing W7-X 'high-mirror' configuration was selected due to its reactor-relevance. The DKES database has been prepared fom a $\beta = 4$ % equilibrium to account for finite beta effects. The dimensionless nature of the DKES approach allows a linear upcscaling of the magnetic configuration. The configuration has been scaled by a factor 3.6 to match a plasma volume of 1400 m^3, which corresponds to a favourable reactor design point found in systems studies with a fusion output of 3 GW. The magnetic field on-axis has been set to 5.5 T accordingly.

Again, a 'standard' flat density profile has been used and kept constant. Also the anomalous electron heat conductivity has again been described by $\chi_e^{ano} \sim 1/n$ and falling off towards the centre with $\chi_e^{\mathrm{edge}} = 2.0$ m^2/s at the very edge.

In Fig. 4 it was shown that the normalised heat flux density $\widehat{Q}$ obtained from the non-linear GENE simulations has the same behaviour and values both for W7-AS and W7-X. In order to derive the stiffness parameter for the ITG critical gradient model some assumption on the normalised heat flux density of the reactor $\widehat{Q}_R$ must be made. In line with the results from Fig. 4 it is assumed that

$$\widehat{Q}_R = \widehat{Q}_{\mathrm{W7X}} = \widehat{Q}_{\mathrm{W7AS}}. \quad (16)$$

With this assumption and gyro-Bohm normalisation it is possible to obtain the stiffness for the Helias reactor with

$$w_{\mathrm{R}} = \left(\frac{a_{\mathrm{W7AS}}}{a_{\mathrm{R}}}\right)^2 \cdot \left(\frac{B_{\mathrm{W7AS}}}{B_{\mathrm{R}}}\right)^2 \cdot \frac{P_{\mathrm{R}}}{P_{\mathrm{W7AS}}} \cdot w_{\mathrm{W7AS}} \approx 1.0 \cdot w_{\mathrm{W7AS}} \quad (17)$$

considering in addition the difference of the magnetic field strength and substituting again the local plasma parameters by the heating power.

Using the stiffness parameter $w_{\mathrm{R}} = 1.0 \cdot w_{\mathrm{W7AS}}$ and also the same critical gradient length as in W7-AS, predictive transport simulations for the reactor scenario were carried out. However, it turned out, that due to the high ion energy flux, the ion temperature profile would decouple at the edge from the electron temperature profile. to achieve similar edge temperature for ions and electrons the anomalous electron heat conductivity was increased by factor five and the simulations repeated. The resulting density and temperature profile of the reactor scenario are shown in Fig. 13.

It can be seen, that in this scenario the anomalous transport dominates over the outer third of the plasma minor radius and the temperature in this region is considerably reduced. The global confinement in this case is $\tau_E^{1D}/\tau_E^{\mathrm{ISS04}} = 1.35$ in terms of the empirical ISS04 scaling. The stiffness cannot be increased much beyond $w_{\mathrm{R}} = 1.0 \cdot w_{\mathrm{W7AS}}$ as otherwise the temperature would shrink further and the fusion output reduced such that the scenario would not be reactor capable anymore if the density is not further increased.

If the stiffness for the reactor scenario could be reduced by a factor two, the temperature towards the edge would stay higher and the confinement would improve from $\tau_E^{1D}/\tau_E^{\mathrm{ISS04}} = 1.35$ to 1.5. Thus, the density could be reduced by nearly 20 % to achieve the same fusion power output.

It remains unclear to what degree the presented scenario for the reactor is an adequate description of the plasma transport under fusion conditions. However, the finding that $w_{\mathrm{R}} = 1.0 \cdot w_{\mathrm{W7AS}}$ is close to an upper limit for the Helias reactor is an important result. Experimental results of W7-X will allow us to draw the connection between W7-AS and W7-X such that the presented model can be validated and further improved. This in turn will allow a further refinement of reactor scenarios.

6. Conclusions and Outlook

In an effort to achieve predictive capability of neoclassical and turbulent transport behaviour in the W7-X experiment on a small computational level, the so far gained understanding of the properties of turbulence in the W7-X magnetic configuration has been reviewed. While the TEM is considered to be strongly stabilized due to the separation of bad curvature and the localisation of the trapped particles, the ITG mode is expected to be a major driver of transport even so it is much more localised on the outboard side of a flux surface than compared to tokamaks.

In order to assess the relevance of these theoretical findings in terms of their applicability to real experiments, the properties of the ITG induced transport in W7-X have been compared to its predecessor W7-AS. For this purpose non-linear gyrokinetic simulations on a full flux surface have, for the first time, been carried out for the W7-AS configuration. While there is qualitative agreement between both devices, the electrostatic potential variations in W7-X are more localised on a thin band on the outboard side of a flux surface than in W7-AS. However, the scaling of the heat flux density normalised by gyro-Bohm values with respect to increase of the ion temperature gradient length (excluding density gradient and radial electric field) is nearly identical in both devices.

In this connection the experimental data of high performance W7-AS discharges has been reviewed where it has been confirmed that the observed anomalous transport shows the typical critical gradient behaviour found in the simulations and scales accordingly with the ion temperature gradient length.

On this basis a simple critical gradient model has been proposed which describes the found behaviour and implemented in a 1-D neoclassical transport code. For verification the code and the model have been applied to W7-AS and good agreement was found where additionally the anomalous electron energy flux was fixed according to an empirical description.

Based on the similarity of the ITG heat flux scaling of W7-AS and W7-X in GENE, the integrated 1-D transport model has been applied for the prediction of the confinement in W7-X. A reactor-relevant scenario with 9 MW NBI power and a density

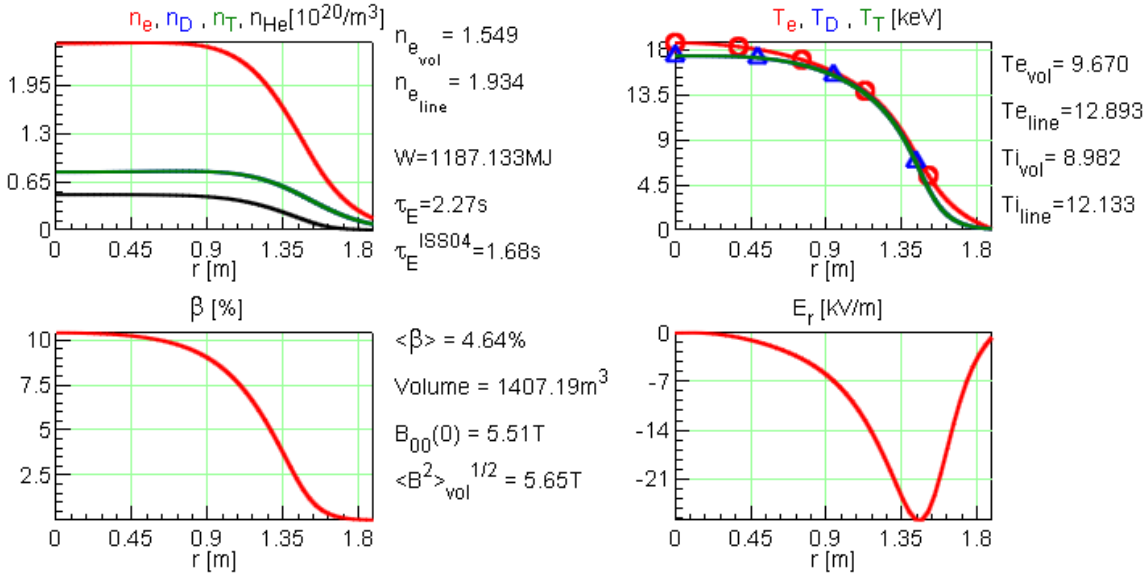

Figure 13: Profiles for the density (left) and temperature (right) for the 1-D predictive transport simulation of the reactor scenario using the same stiffness as in W7-AS and W7-X as well as an increased anomalous electron heat conductivity.

of $1 \cdot 10^{20}$ m^{-3} was simulated and found, that even with the ITG model the global confinement improvement with respect to the empirical ISS04 scaling is retained with a confinement improvement factor of $\tau_E^{1D}/\tau_E^{\mathrm{ISS04}} = 1.7$. A sensitivity analysis showed that a factor two increase of the stiffness decreases the confinement improvement to a factor 1.4 while a reduction of the stiffness by a factor two increases the confinement to 1.9.

Finally, the same methodology was applied to a Helias reactor scenario using again the same critical gradient length and stiffness parameters as in W7-AS and W7-X. The anomalous electron heat flux density was increased in order to prevent a decoupling of the electron and ion temperature at the edge. But even with the ITG induced transport and the increase electron transport a suitable reactor solution is found with a global confinement improvement of 1.35 with respect to the ISS04 scaling. However, the stiffness can in this reactor scenario not be increased very much as otherwise the reduction of the ion temperature would reduce the fusion power output which can only to some degree be compensated by an increase of the density.

Finally, it should be noted that although the introduced ITG model is rather basic, this work represents the first attempt to include first-princpile physics motivated models for the prediction of turbulent transport in integrated plasma scenarios. In the next steps, it is foreseen to include both the effect of the density gradient as well as the electric field which are anticipated to reduce ITG turbulence. It will also be investigated to what degree modes can be considered which drive electron transport.

7. Acknowledgments

This work has been carried out within the framework of the EUROfusion Consortium and has received funding from the Euratom research and training programme 2014-2018 under grant agreement No 633053. The views and opinions expressed herein do not necessarily reflect those of the European Commission.

References

[1] B. J. Green. "ITER: burning plasma physics experiment." *Plasma Physics and Controlled Fusion*, vol. 45, p. 687 (2003).
[2] G. Grieger and I. Milch. "Das Fusionsexperiment WENDELSTEIN 7-X." *Physikalische Bltter*, vol. 49, p. 1001 (1993).
[3] M. Hirsch, J. Baldzuhn, C. D. Beidler et al. "Major results from the stellarator Wendelstein 7-AS." *Plasma Physics and Controlled Fusion*, vol. 50, p. 053001 (2008).
[4] H. Yamada, J. H. Harris, A. Dinklage et al. "Characterization of energy confinement in net-current free plasmas using the extended International Stellarator Database." *Nuclear Fusion*, vol. 45, p. 1684 (2005).
[5] F. Warmer, C. Beidler, A. Dinklage et al. "Limits of Confinement Enhancement for Stellarators." *Fusion Science and Technology*, vol. 68 (2015).
[6] C. D. Beidler, K. Allmaier, M. Y. Isaev et al. "Benchmarking of the mono-energetic transport coefficients - results from the International Collaboration on Neoclassical Transport in Stellarators (ICNTS)." *Nuclear Fusion*, vol. 51, p. 076001 (2011).
[7] P. Xanthopoulos, F. Merz, T. Grler et al. "Nonlinear Gyrokinetic Simulations of Ion-Temperature-Gradient Turbulence for the Optimized Wendelstein 7-X Stellarator." *Physical Review Letters*, vol. 99, p. 035002 (2007).
[8] J. H. E. Proll, P. Helander, J. W. Connor et al. "Resilience of Quasi-Isodynamic Stellarators against Trapped-Particle Instabilities." *Physical Review Letters*, vol. 108, p. 245002 (2012).
[9] P. Helander, T. Bird, F. Jenko et al. "Advances in stellarator gyrokinetics." *Nuclear Fusion*, vol. 55, no. 5, p. 053030 (2015).
[10] J. H. E. Proll, P. Xanthopoulos and P. Helander. "Collisionless microinstabilities in stellarators. II. Numerical simulations." *Physics of Plasmas*, vol. 20, p. 122506 (2013).
[11] F. Jenko, W. Dorland, M. Kotschenreuther et al. "Electron temperature gradient driven turbulence." *Physics of Plasmas*, vol. 7, p. 1904 (2000).
[12] P. Xanthopoulos, W. A. Cooper, F. Jenko et al. "A geometry interface for gyrokinetic microturbulence investigations in toroidal configurations." *Physics of Plasmas*, vol. 16, p. 082303 (2009).
[13] T. Görler, X. Lapillonne, S. Brunner et al. "The global version of the gyrokinetic turbulence code {GENE}." *Journal of Computational Physics*, vol. 230, no. 18, p. 7053 (2011).
[14] P. Xanthopoulos, H. Mynick, P. Helander et al. "Controlling Turbulence in Present and Future Stellarators." *Physical Review Letters*, vol. 113, p. 155001 (2014).

[15] J. Baldzuhn, M. Kick, H. Maassberg et al. "Measurement and calculation of the radial electric field in the stellarator W7-AS." *Plasma Physics and Controlled Fusion*, vol. 40, no. 6, p. 967 (1998).

[16] S. Toda, M. Nunami, A. Ishizawa et al. "How to apply a turbulent transport model based on a gyrokinetic simulation for the ion temperature gradient mode in helical plasmas." *Journal of Physics: Conference Series*, vol. 561, no. 1, p. 012020 (2014).

[17] H. Maaßberg, R. Brakel, R. Burhenn et al. "Transport in stellarators." *Plasma Physics and Controlled Fusion*, vol. 35, p. B319 (1993).

[18] U. Stroth. "A comparative study of transport in stellarators and tokamaks." *Plasma Physics and Controlled Fusion*, vol. 40, p. 9 (1998).

[19] Y. Turkin, H. Maaßberg, C. D. Beidler et al. "Current Control by ECCD for W7-X." *Fusion Science and Technology*, vol. 50, p. 387 (2006).

[20] Y. Turkin, C. D. Beidler, H. Maaßberg et al. "Neoclassical transport simulations for stellarators." *Physics of Plasmas*, vol. 18, p. 022505 (2011).

[21] W. I. van Rij and S. P. Hirshman. "Variational bounds for transport coefficients in threedimensional toroidal plasmas." *Phyiscs of Fluids B: Physics of Plasmas*, vol. 1, p. 563 (1989).

[22] S. P. Hirshman, K. C. Shaing, W. I. van Rij et al. "Plasma transport coefficients for nonsymmetric toroidal confinement systems." *Physics of Fluids*, vol. 29, p. 2951 (1986).

[23] H. Maaßberg, C. D. Beidler and E. E. Simmet. "Density control problems in large stellarators with neoclassical transport." *Plasma Physics and Controlled Fusion*, vol. 41, p. 1135 (1999).